JNPS 10 (2): 41-58 (2024)
ISSN: 2392-473X(Print), 2738-9537 (Online)

Research Article *©Nepal Physical Society*
doi.org/10.3126/jnphyssoc.v10i2.79475

Theoretical Evaluation on Electronic and Biological Properties of Quercetin by Quantum Chemical and Molecular Docking Method

Tirth Raj Paneru[a,d], Poonam Tandon[b], Bhawani Datt Joshi[c*]

[a]*Department of General Science, Far Western University, Kanchanpur,Mahendranagar, 10400, Nepal*
[b]*Department of Physics, University of Lucknow, Lucknow-226007, India*
[c]*Department of Physics, Siddhanath Science Campus, Tribhuvan University, Mahendranagar, 10400, Nepal*
[d]*Central Department of Physics, Tribhuvan University, Kirtipur, Kathmandu, Nepal*
**Corresponding author: bhawani.joshi@snsc.tu.edu.np,pbdjoshi@gmail.com (B.D. Joshi)*

Submitted: October 25, 2024; **Revised:** May 24, 2025; Acceped: June 01, 2025

Abstract

The quantum chemical method was used to present the electronic and biological properties of quercetin by enlightening specific reactive sites on the molecule, which demonstrated intra- and intermolecular hydrogen bonding. The geometrical parameters (bond lengths and bond angles) of quercetin were determined and compared to the experimental structure of monohydrate quercetin. The strong intra-molecular hydrogen bond O3-H29…O4 was justified by the quantum theory of atoms in molecules, which was also confirmed by the RDG scatter plot and isosurface. With the global minimum potential at O4 and maximum potential at H31, two groups, OH and C=O, have been investigated as the location for intermolecular hydrogen bonding for solid-state conformation and biological activity. The HOMO–LUMO gap in gaseous and solvent ethanol was measured to be 3.777 eV and 3.932 eV, respectively, confirming that quercetin is more kinetically stable in gaseous medium than solvent ethanol. Global reactivity descriptors provide additional information about the chemical behavior of quercetin in the gaseous and solvent phases. Toxicity measurement predicts that the title molecule will exhibit a third class of toxicity. Molecular docking with the protein aldose reductase reveals that quercetin has the highest binding affinity and the lowest inhibition constant, with the target protein codes 2BGS and 2VDS confirming that it may inhibit aldose reductase.

Keywords: Quercetin, QTAIM, HOMO–LUMO, ADMET, Molecular docking

1. Introduction

Flavonoids are naturally occurring phenol derivatives in natural products like plants, fruits, and vegetables have antioxidant potential [1]. Flavonoids have anti-inflammatory properties that may improve vascular function [2]. Quercetin is a flavone that can be found in a variety of foods, including vegetables, fruits, red wine, olive oil, and tea [3]. Quercetin is pentahydroxyflavone with molecular

formula $C_{15}H_{10}O_7$, and its IUPAC name is 2-(3,4-dihydroxyphenyl)-3,5,7-trihydroxychromen-4-one [4]. Free radicals in quercetin play a key role in the onset of many diseases, including metabolic syndrome, hypertension, and vascular disorders. Due to antioxidant properties, it prevents the molecules that produce free radicals from oxidation [5]. Plants contain quercetin in the form of glycone or carbohydrate conjugates. Quercetin has many health benefits, such as protecting the cardiovascular system, exhibiting antitumor and anticancer properties, relieving allergy symptoms, assisting in the management of diabetes, and having gastroprotective properties [6]. The study of this molecule is an area of interest for exploration because of the multitude of diverse biological activities.

Dhaouadi et al. investigated the interaction of quercetin with hydroxyl radicals and superoxide radicals and found a correlation between structural alteration and antioxidant activity [7]. Jeevitha et al. investigated the activity of a glycosyl group attached to a different ring of quercetin and discovered that ring A is more antioxidant than another [8]. To assess its stability, the molecular structure of quercetin on single-layer graphene was analyzed using DFT with the 6–21 basis set, and global reactivity parameters were examined [9]. Karmakar and Singh examined the hydrogen bonding interactions of quercetin as a donor with selected acceptor molecules using spectroscopic and DFT methods, confirming multiple hydrogen bonding interactions between quercetin and the acceptor molecules. [10]. The interaction of quercetin with the S-glycoprotein of SARS-CoV-2 was carried out by Aljelehawy et al. and found to be well bound with the active sites of the receptor [11].

The literature shows that the investigation of the electronic and molecular properties of the title molecule by identifying its reactive sites using DFT has not been explored yet. We performed quantum chemical calculations for this work using the B3LYP hybrid functional with basis set 6–311++G(d,p) and density functional theory. The benchmarking report supported the claim that the hybrid functional B3LYP outperforms other functional, including WB97XD, in terms of electronic and vibrational results [12]. The basis set 6-311++G(d,p) contains diffuse and polarized functions. The B3LYP/6-311++G(d,p) level of theory elevates accuracy for structural parameters, ground state energies, and vibrational frequencies for illustrating electronic properties [13,14]. This work emphasizes the precise locations of electrophiles and nucleophiles by indicating the values of electrostatic potential on molecular electrostatic potential surfaces. The nucleophilic and electrophilic sites of the molecule interact with the targeted protein, aldose reductase, allowing for an evaluation of the biological performance of the title compound elucidated from molecular docking. This work also identifies the exact location of intermolecular interaction for the crystal packing of the title molecule. The intra- and intermolecular hydrogen bonding interactions in the molecule are highlighted using various approaches, including QTAIM analysis and non-

covalent interaction analysis. The chemical hardness, softness, and electrophilicity index of the molecule are also evaluated for the prediction of reactivity and stability. Moreover, the drug-like properties of the title molecule are examined. The chemical structure of quercetin is shown in Figure 1.

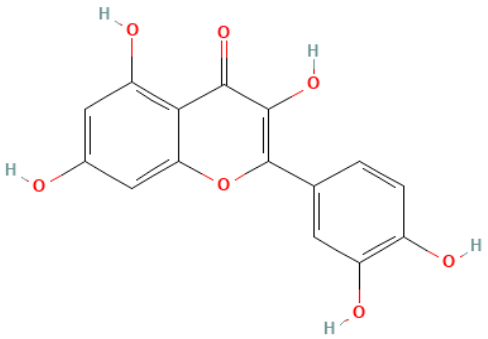

Figure 1. Chemical structure of quercetin.

2. Materials and Methodology

To begin the study of a molecule, its optimized structure is required, which was achieved using density functional theory with the Gaussian 09 software package [15,16]. The quantum chemical computations were performed utilizing the B3LYP hybrid functional in conjunction with the 6–311++G(d,p) basis set, which contains polarization and diffusion functions [17,18]. The QTAIM method, which was implemented by the AIMALL (10.05.04) software package, was used to assess the strength of intra-molecular hydrogen bonding interactions [19,20]. For the visualization of the highest occupied molecular orbital (HOMO), lowest unoccupied molecular orbital (LUMO), and optimized structure of the molecule, GaussView 05 was used [21] . Non-covalent interactions in the RDG scatter plot and its isosurface, which show interactions and extrema on the molecular electrostatic potential surface, were rendered using Multiwfn 8 and VMD1.9.4 software. [22,23]. GaussSum 3.0 software was utilized to generate the DOS spectrum of the molecule occurring in both the solvent and gaseous phases [24]. ADMET properties of the title molecule were evaluated by using SwissAdme and ProTox 3.0 web tool [25,26]present in drugs, food, environments, and consumer goods, is an integral part of our everyday life. However, depending on the amount and duration, such interactions can also result in adverse effects. With the increase in computational methods, the in silico methods can offer significant benefits to both regulatory needs and requirements for risk assessments and the pharmaceutical industry to assess the safety profile of a chemical. Here, we present ProTox 3.0, which incorporates molecular similarity and machine-learning models for the prediction of 61 toxicity endpoints such as acute toxicity, organ toxicity, clinical toxicity, molecular-initiating events (MOE. The title molecule was docked with enzyme aldose reductase using AutoDock tools (1.5.4), and the binding sites were visualized with Discovery Studio Visualizer 4.5 [27,28].

3. Results and Discussion

3.1 Optimized structural parameters

The optimized structure of quercetin with atom numbering is depicted in Figure 2. The ground state energy of the optimized structure of quercetin calculated at B3LYP/6–311++G(d,p) level of theory was found to be –693084.99 kcal/mol.

The calculated optimized structural parameters (bond length and bond angle) for the quercetin were compared with corresponding experimental value of bond length and angle in the monohydrate quercetin [29]the world's repository for small molecule crystal structures. The entry contains experimental data from a crystal diffraction study. The deposited dataset for this entry is freely available from the CCDC and typically includes 3D coordinates, cell parameters, space group, experimental conditions and quality measures.","DOI":"10.5517/CCWBKLB", "language":"en","medium":"CIF", "publisher":"Cambridge Crystallographic Data Centre","source":"DOI.org (Datacite. The calculated values of bond length of O4-C13, O3-H29, O6-C20, and C12-C13 were found to differ from experimental values by 0.032, 0.026, 0.021, and 0.029 Å, respectively. On the other hand, bond angles C12-O2-H28, O2-C12-C10, C8-C13-C12, O6-C20-C22, O7-C22-C20, and O7-C22-C21 deviated from the experimental values by 3.1, 2.3, 2.2, 2.4, 3.2, and 3.3˚, respectively. Except for those mentioned bonds and angles, the calculated bond length and bond angles were found to be in good agreement with corresponding experimental values. The slight difference in calculated data occurred because, in the experimental structure, monohydrate was used for quercetin crystal packing and intra- and intermolecular hydrogen bonding between the OH and C=O groups was considered, whereas our theoretical calculation was performed in a gaseous state and only for a single quercetin.

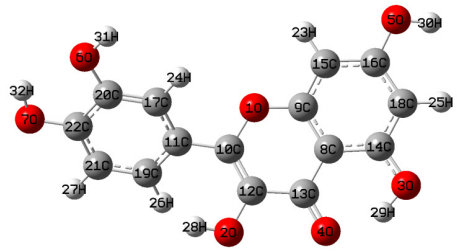

Figure 2. The optimized structure of quercetin with leveling on atoms.

3.2 Atoms in molecule (AIM) analysis

Atoms in molecules are studied by analyzing their electronic structure, including chemical bonds and electron density distribution, by focusing on critical points based on the quantum theory of atoms in molecules. This also allows for an assessment of the strength and nature of intra- and intermolecular hydrogen bonding [30]. The total electron density (H_{BCP}), which is the sum of the kinetic (G_{BCP}) and potential energy (V_{BCP}) densities, and the Laplacian of electron density (ρ_{BCP}) are used to define the type of hydrogen bonding. If the total van der Wall radii (r_H+ r_A) of the interacting atoms are larger than the distance between them, then the van der Wall interaction between those atoms is possible [14]. The topological parameters for subsequent intra-molecular hydrogen bonding and the geometrical

parameters for donors and acceptors are presented in Tables 1 and 2, respectively. Figure 3 displays the molecular graph that illustrates the intra-molecular hydrogen bonding in quercetin. In quercetin, $\rho_{BCP} > 0$) and ($H_{BCP} < 0$), indicate that the hydrogen bond is medium and partially covalent in nature [31]. Two intra-molecular hydrogen bonds, O2-H28…C19 and O3-H29…O4 were detected in quercetin, and the interaction energy for the H29…O4 was computed to be –14.499 kcal/mol, which is the strongest hydrogen bonding. The bond ellipticity and bond length for interaction H28…C19 were found to be higher, indicating that it is a weak interaction. For interaction H29…O4, the bond length and bond angle were calculated to be 1.698 Å and 148.59˚, respectively. These values are in good agreement with the corresponding experimental values of 1.712 Å and 152.2˚, respectively.

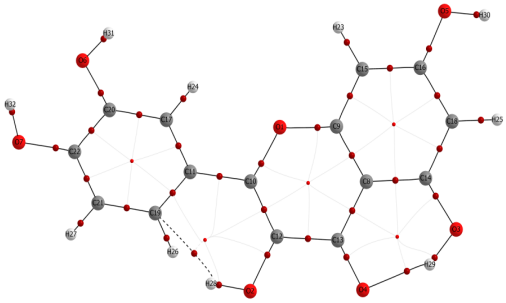

Figure 3. Topological mapping showing intra-molecular interactions in the molecular graph of quercetin.

Table. 1. The topological parameters for intra-molecular interactions: electron density (ρ_{BCP}), Laplacian of electron density (ρ_{BCP}), total electron density (H_{BCP}), interaction energy (E_{int}), kinetic energy density (G_{BCP}), potential energy density (V_{BCP}), bond ellipticity (ε) and geometrical bond length for quercetin.

Interactions	H29…O4	H28…C19
Bond length	1.698	2.420
ρ_{BCP}	0.04864	0.01281
G_{BCP}	–0.00607	–0.00181
V_{BCP}	–0.04621	–0.00791
ρ_{BCP}	0.13625	0.04617
H_{BCP}	–0.05228	–0.00972
E_{int}	–14.499	–2.482
ε	0.0134	1.5376

Table 2. Bond length and bond angle, as well as the total of the van der Waal radii ($r_H + r_A$) for intra-molecular interactions in quercetin.

D-H...A	O3-H29…O4	O2-H28…C29
D-H (A)	0.993	0.965
H...A (A)	1.698	2.420
D-H...A ()	148.59	124.01
($r_H + r_A$) (A)	2.72	3.22

3.3. Non covalent interaction

The non-covalent interactions provide a strong foundation for distinguishing hydrogen bond interactions, van der Walls interactions, and steric repulsion using the RDG scatter plot and isosurface plot generated by Multiwfn and VMD software [32]. The value of RDG can be determined by the following equation [33].

$$RDG(r) = \frac{1}{2(3\pi^2)^{\frac{1}{3}}} \frac{|\nabla\rho(r)|}{\rho(r)^{\frac{4}{3}}}$$

Here, is the gradient of electron density and is the electron density. The type of interactions is distinguished by the graph that is plotted between sign$\lambda_2(\rho)$, the second

eigen value of electron density, and RDG. As represented by the RDG isosurface in Figure 4 (b), the green color spike represents van der Wall interaction with signλ2(ρ) = 0, signλ2(ρ) < 0, and signλ2(ρ) > 0, represented by blue and red color, which stands for hydrogen bond interaction and steric repulsion [34]. The RDG graph and its isosurface for the title molecule are shown in Figure 4 (a) and (b), respectively. The spikes that appeared in the range of –0.03 to –0.05 a.u., indicated the presence of a strong intra-molecular hydrogen bond, O3-H29…O4, which was further supported by AIM analysis in section 3.2. The red spikes show up almost between 0.01 and 0.05 a.u. and indicate that there was significant steric repulsion between the oxygen and in the ring of the molecule.

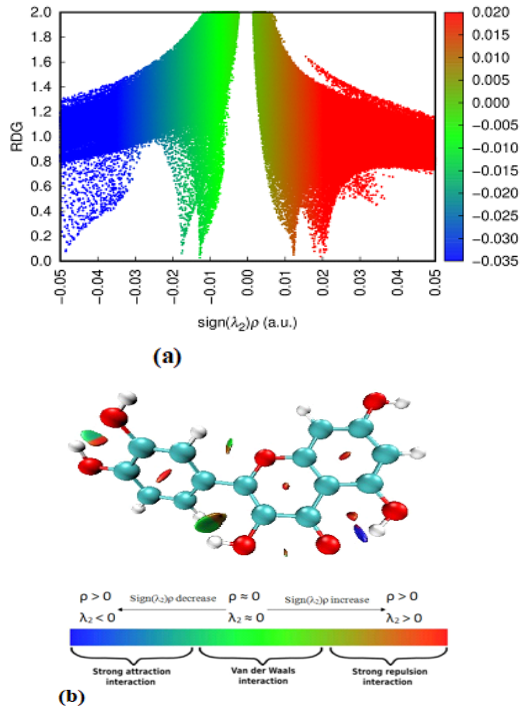

Figure 4. (a) The RDG scatter plot and (b) isosurface showing non-covalent interactions in quercetin.

3.4 Electrostatic potential (ESP) surface analysis

Electrostatic potential is a fundamental concept for predicting electron-rich and electron-poor regions, as well as identifying electrophilic and nucleophilic sites in molecules [35]. The total contributions from all of the nuclei and electrons in the system are typically used to express the electrostatic potential at a point in a molecular system given by the relation: [36]

$$V^{ES}(\overrightarrow{r}) = \sum_{A} \frac{Z_A}{|\vec{R}_A - \vec{r}|} - \int \frac{\rho(\vec{r}')d\vec{r}'}{|\vec{r}' - \vec{r}|}$$

Where Z_A is a charge on the nucleus with location and is the electron density function.

The molecular surface has a negative potential in the red color region, a positive potential in the blue region, and a neutral region represented by green color [37]. The blue and orange dots at the extrema of the ESP surface represent negative and positive potential, respectively [38]. The electrostatic potential surface for quercetin with the value of electrostatic potential is shown in Figure 5. The highest positive potential of 65.31 kcal/mol is associated with the H31 of the O–H group, and the lowest negative potential of –47.80 kcal/mol is attributed to O4 of the C=O group. Hence, O4 and H31 in quercetin have been identified as the best nucleophile and electrophile, respectively, and serve as ideal sites for intermolecular interaction for biological activity and crystal packing. Similarly, the atoms H23, H26, H28, H30, and H32 have positive electrostatic

potential and should be targeted by nucleophiles. The atoms O1, O2, O3, O5, O6, and O7 have a negative potential as nucleophiles and are prone to electrophilic attack. These atoms should be involved in biological interactions as well as intra- and intermolecular interactions.

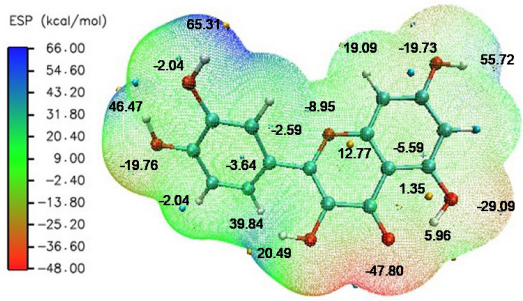

Figure 5. ESP mapped molecular vdW surface of quercetin.

3.5 Frontier molecular orbital and density of state

The energy associated with the highest occupied molecular orbital represents the ionization potential, whereas the energy associated with the lowest unoccupied molecular orbital represents the electron affinity. HOMO represents an electron-donating group, whereas LUMO accepts them. The energy gap between HOMO and LUMO, also known as the band gap, determines chemical stability and reactivity [39,40]. LUMO accepts electrons, and HOMO donates them. The density of state provides a thorough understanding of molecular structure by visualizing the distribution of molecular orbitals at various energy levels. The simultaneous effects of the donor and acceptor groups on electron delocalization result in the DOS spectrum [41]. The HOMO–LUMO plot and the DOS spectrum for quercetin in gaseous medium and solvent ethanol are shown in Figure 6. Quercetin was found to have an energy gap of 3.977 and 3.932 eV between its HOMO and LULO in gaseous medium and solvent ethanol, respectively. This suggests that quercetin is more reactive in solvent ethanol and more stable in a gaseous medium. Quercetin is more polarizable in solvent ethanol because it allows charge transfer more easily. The energy gap in the HOMO–LUMO plot was found to be identical to that in the DOS spectrum. Another flavonoid, cirsilineol, has an energy gap of 3.973 eV in gas and 3.222 eV in solvent ethanol, indicating that the energy gap in gaseous medium is nearly identical, but quercetin has slightly higher stability in solvent ethanol than cirsilineol [14]. The higher intensity of the DOS spectrum at certain energy levels suggests that there are multiple states of occupation; the red and green lines in the spectrum represent virtual orbitals and occupied orbitals, respectively. The positive value in the spectrum denotes bonding interaction, while the negative value represents antibonding interaction [42].

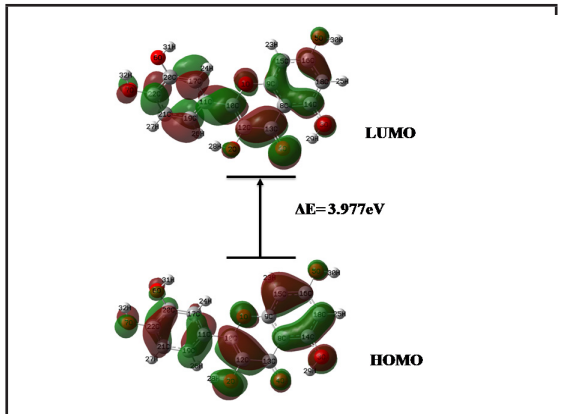

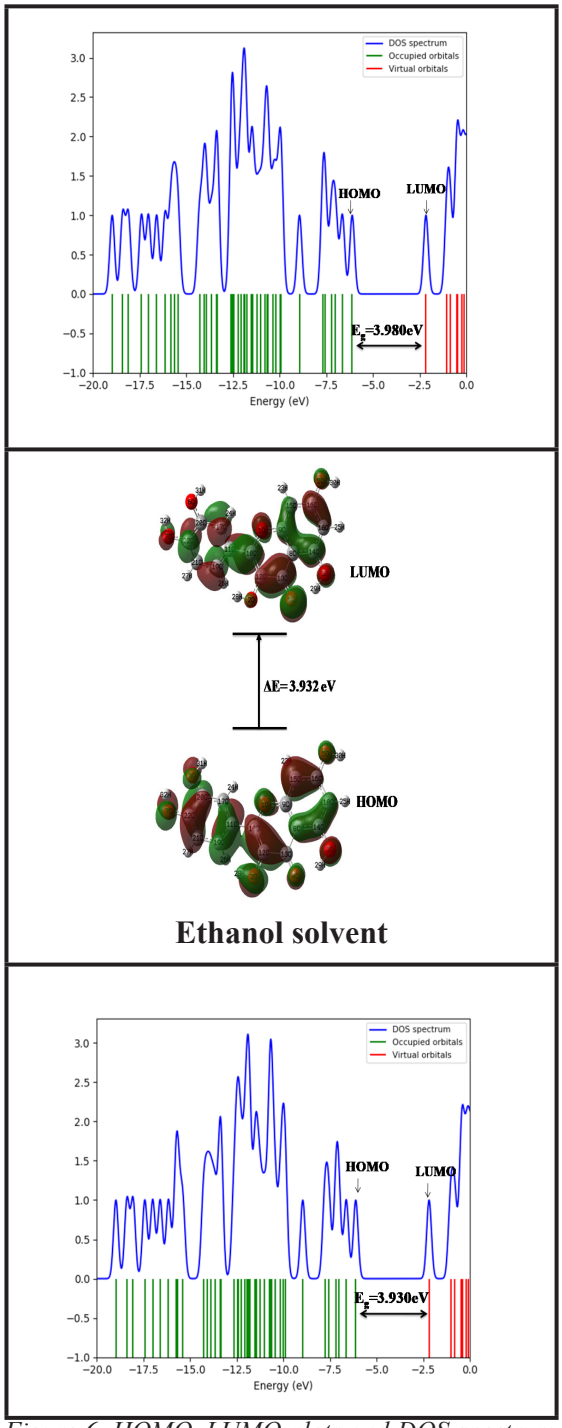

Figure 6. HOMO–LUMO plots and DOS spectrum for the quercetin in gaseous and solvent ethanol.

3.6 Global reactivity descriptors

Global reactivity descriptors refer to a variety of quantities other than the energy gap that are more important for predicting the behavior of chemical species. The many global reactive descriptors provided by Koopman in terms of ionization potential and electron affinity, such as electronegativity , chemical softness , hardness , and electrophilicity index (, provide theoretical insight into chemical behavior [43]. The formula for those mentioned reactivity descriptors is as follows: [44,45]

$$\text{Electronegativity } (\chi) = \frac{1}{2}(I + A)$$

$$\text{Chemical Potential } (\mu) = -\chi = -\frac{1}{2}(I + A)$$

$$\text{Global Hardness } (\eta) = \frac{1}{2}(I - A)$$

$$\text{Softness}(S) = \frac{1}{2\eta}$$

$$\text{Global Electrophilicity index}(\omega) = \frac{\mu^2}{2\eta}$$

The reactivity descriptors computed for the quercetin in gaseous medium and in solvent ethanol are presented in Table 3. Quercetin was found to have a higher ionization potential and electron affinity in solvent ethanol when compared to gaseous medium. This suggests that it functions better as an electron acceptor in solvent and as an electron donor in gaseous medium. Quercetin exhibited a higher global softness and electrophilicity index in the solvent ethanol phase compared to the gaseous medium. This suggests that the solvent exhibits stronger electrophilic

properties and facilitates intra-molecular charge transfer.

Table. 3. Global reactivity descriptors of quercetin.

Medium	Gaseous	Ethanol
I(eV)	6.0997	6.1179
A(eV)	2.1230	2.1861
(I– A)(eV)	3.9767	3.9318
(eV)	4.1114	4.1520
(eV)	–4.1114	–4.1520
(eV)	1.9884	1.9659
S(eV^{-1})	0.2515	0.2543
(eV)	4.2506	4.3845
ΔNmax	2.0677	2.1120

3.7 Mulliken charge analysis

Mulliken atomic charges reveal information about a chemical system's dipole moment, electron distribution, and polarizability, providing insights into its electronic structure and behavior. It also helps to provide information on chemical reactivity and interactions [46]. Figure 7 displays the atomic charges computed on each quercetin atom at the B3LYP/6–311++G(d,p) level of theory. All the hydrogen of quercetin has positive charges, whereas all oxygen contains negative charges except O1, which has a small positive charge. Carbons C11 and C18 have positive charges, but C10, C12, C13, C14, C15, C16, C17, C19, C20, C21, and C22 have negative charges, as predicted by Mulliken's charge analysis. The atoms with the highest positive and negative charges were C11 and C15, respectively.

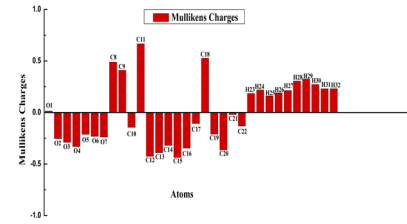

Figure 7. Distribution of Mulliken charges quercetin molecule.

3.8 ADMET properties analysis

ADMET standards are used to evaluate pharmacokinetic properties and provide information on the safety of title molecules as drug candidates. Predicting pharmacokinetic and drug–like properties is necessary for the evaluation of newly discovered drugs [47]. Table 4 displays the pharmacokinetic and drug-like properties of quercetin as determined by the SwissAdme web tool. With a molecular weight of less than 500 g/mol, an H–bond donor of less than 5, an H–bond acceptor of less than 10, a number of rotatable bonds less than 10, lipophilicity less than 5, molar refractivity within the range of 40–130, and a polar surface area less than 140 $Å^2$, it implied that five rules given by Lipinski not violated. Hence, quercetin exhibits drug–like properties [48]. The LD50 value for quercetin as detected by the ProTox–II web tool shows that it falls within the range of (50 < LD50 < 300) which indicates that it is class III toxic if swallowed. The boiled egg diagram and radar plot for title molecule to access bioavailability are shown in Figure 8. The red dots in the white area of the boiled egg model show that quercetin is absorbed by the gastrointestinal system, increasing its bioavailability. Regarding the radar plot, quercetin has excellent

bioavailability because, aside from molecule instauration, other parameters for assessing bioavailability lie inside the pink area.

Table 4. The different ADMET parameters for quercetin.

Parameters	Values
Molecular weight (g/mol)	302.24
Rotatable bond	1
Hydrogen bond acceptor	7
Hydrogen bond donor	5
Topological polar surface area (Å^2)	131.36
Molar refractivity	78.03
Blood brain–barrier permeate	No
P–glycoprotein substrate	No
Lipophilicity (WlogP)	1.99
Water solubility (log *S)*	–3.16
Permeability coefficient (log Kp cm/s)	–7.05
Lipinski violations	0
GI absorption	High
Synthetic accessibility	3.23
Bioavailibility score	0.55
Lethal Dose (LD 50)	159mg/kg

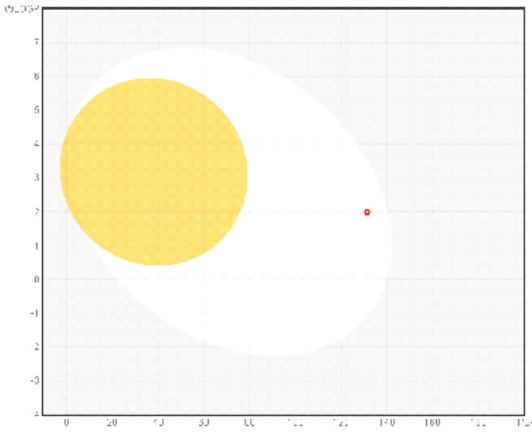

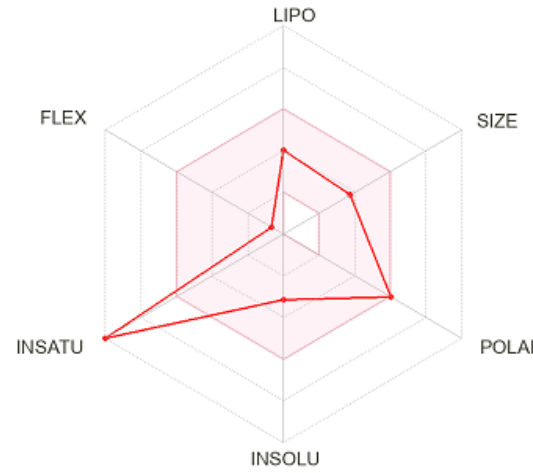

Figure 8. Swiss ADME boiled egg model and radar model for the bioavailability of quercetin.

3.9 Molecular Docking

Molecular docking is a computational method that forecasts the interaction between a protein acting as a receptor and a ligand acting as a drug molecule, assessing the strength of the interaction through binding affinity [49]. Swiss target selection was used to achieve the target protein for molecular docking [50]. The aldose reductase protein has been selected for molecular docking, as shown by its higher probability predicted from the Swiss Target Prediction. Aldose reductase inhibitors have been studied for their ability to reduce the accumulation of sorbitol, thereby preventing secondary diabetic complications [51]neuropathy, nephropathy and cataractogenesis. Subsequently, several AR inhibitors have been developed and tested for diabetic complications. Although these inhibitors have found to be safe for human use, they have not been successful in clinical studies because of limited efficacy. Recently, the potential physiological role

of AR has been reassessed from a different point of view. Diverse groups suggested that AR, in addition to reducing glucose, also efficiently reduces oxidative stress-generated lipid peroxidation-derived aldehydes and their glutathione conjugates. Because lipid aldehydes alter cellular signals by regulating the activation of transcription factors such as NFkB and AP1, inhibition of AR could inhibit such events. Indeed, a wide array of recent experimental evidence indicates that the inhibition of AR prevents oxidative stressinduced activation of NF-kB and AP1 signals that lead to cell death or growth. Furthermore, AR inhibitors have been shown to prevent inflammatory complications such as sepsis, asthma, colon cancer and uveitis in rodent animal models. The new experimental in vitro and in vivo data has provided a basis for investigating the clinical efficacy of AR inhibitors in preventing other inflammatory complications than diabetes. This review describes how recent studies have identified novel plethoric physiological and pathophysiological significance of AR in mediating inflammatory complications, and how the discovery of such new insights for this old enzyme could have considerable importance in envisioning potential new therapeutic strategies for the prevention or treatment of inflammatory diseases.","container-title":"BioMolecular Concepts","DOI":"10.1515/bmc.2011.002","ISSN":"1868-503X, 1868-5021","issue":"1-2","language":"en","license":"http://creativecommons.org/licenses/by-nc-nd/3.0/","page":"103-114","source":"DOI.org (Crossref. We obtained the protein codes 2VDG and 2BGS from the protein data bank, and we used them to perform molecular docking [52]. To begin molecular docking, the water molecules were removed from the protein and Kollmann charges added to it. Protein active sites were identified using a grid box of 60Å x 60Å x 60Å with a spacing of 0.375Å. The interactions with the location of binding sites of protein codes 2VDG and 2BGS are shown in Figure 9. The binding affinity, residues, bond length, inhibition constant, and efficiency of interaction are presented in Table 5.

The binding sites for the PDB codes 2BGS and 2VDS were predicted within a grid box with coordinates of x = 44.349, y = 53.843, and z = 17.213. The results indicate that the binding affinity of the title molecule with 2BGS and 2VDS was found to be –10.9 and –10.7 kcal/mol, respectively, which is higher than that of cirsilineol [14]. The atoms O6, H31, O7, O2, and H28 of quercetin form hydrogen bonds with the residues TYR60, GLN188, ASP55, THR31, SER215, and ILE257. Moreover, 2VDS has H–bonds residues are LYS88, ASP55, and THR31 with the atoms O6, H32, and O7, respectively. This could also imply that the reactive region identified by molecular electrostatic potential surface analysis of the title molecule participated in biological activities with the targeted protein aldose reductase. The inhibition constant for both protein codes was lowest with highest binding affinity, and the RMSD between initial structure and docked structure was < 2, indicating quercetin inhibits aldose reductase.

Table 5. Molecular docking parameters of quercetin with protein code (2BGS and 2VDG) of aldose reductase.

Selected PDB code and their resolution	Binding Affinity (kcal/mol)	H–Bond residues	Atoms	Bond length (Å)	Ligand efficiency	Inhibition constant (μM)	RMSD (Å)
2BGS (1.64 Å)	–10.9	TYR60	O6	1.92	0.50	0.010	1.39
		GLN188	H31	2.58			
		ASP55	H31	2.34			
		THR31	O7	2.47			
		SER215	O2	2.68			
		ILE257	H28	2.04			
2VDS (1.92 Å)	–10.7	LYS88	O6	2.74	0.49	0.014	1.41
		ASP55	H32	2.52			
		THR31	O7	2.34			

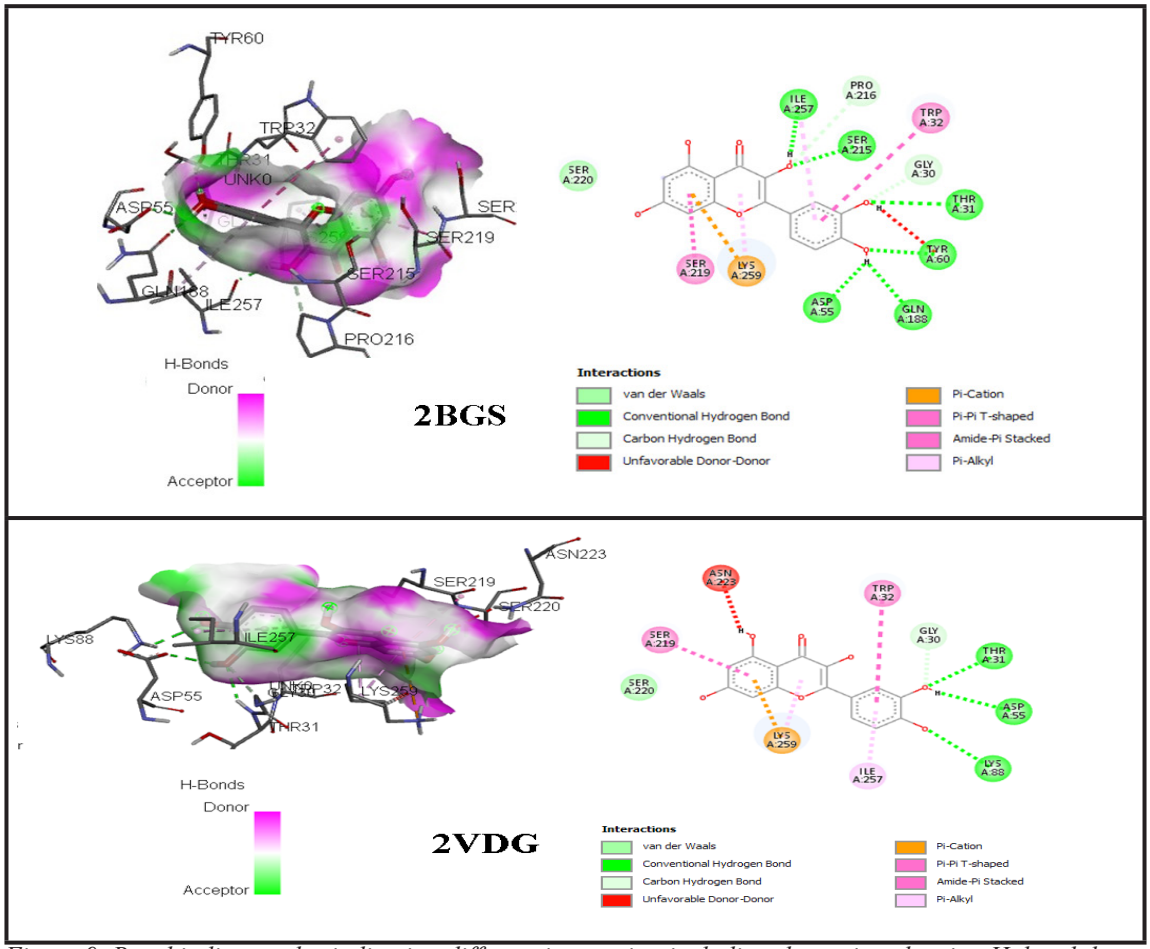

Figure 9. Best binding modes indicating different interaction including the region showing H–bond donor acceptor.

4. Conclusion

The electronic and biological properties of quercetin were highlighted in this study using quantum chemical calculations. The ground state optimized energy, computed at the B3LYP/6–311++G(d,p) level of theory, was –693084.99 kcal/mol. Except for intra- and intermolecular hydrogen bonding sites, the bond angles and lengths were found to be in good agreement with those of monohydrate quercetin. Two intra-molecular hydrogen bonds were investigated by QTAIM analysis, among them H29… O4 was the strongest hydrogen bond with an interaction energy of –14.499 kcal/mol. The RDG surface isosurface provides additional support for the intra-molecular hydrogen bonding. The highest positive value of electrostatic potential of 65.31 kcal/mol and –47.80 kcal/mol justified the exact location of intermolecular hydrogen bonding at O4 as a nucleophile and H31 as an electrophile, which may play a role in the crystal packing of the title molecule as well as for the biological action. Quercetin was found to be more reactive and polarizable in solvent ethanol than in gaseous medium. Global reactive descriptors were evaluated in gaseous and solvent ethanol and revealed that quercetin is softer in solvent. The atoms C11 and C15 contain the highest positive and negative charges, respectively. According to ADMET analysis, quercetin is absorbed by the gastrointestinal system, which confirmed that it has excellent bioavailability. Quercetin inhibits aldose reductase with the highest binding affinity of –10.9 kcal/mol to the protein code 2BGS.

Conflict of interest

There are no conflicts to declare.

Author contributions

T. R. Paneru: Conceptualization of research activity, investigation, data analysis, writing original Draft, and formal analysis; P. Tandon: Software and supervision; B.D. Joshi: Writing-review, editing, and supervision.

Ethical issue

The authors declare no ethical issues.

Acknowledgments

T.R. Paneru acknowledges the University Grants Commission (UGC), Nepal, for granting a partial research fellowship (UGC Award No. PhD-079/80-ST-18), and also acknowledges Far Western University, Kanchanpur, Nepal.

References

[1] P.C.H. Hollman, J.M.P. Van Trijp, M.N.C.P. Buysman, M.S. V.D. Gaag, M.J.B. Mengelers, J.H.M. De Vries, M.B. Katan, Relative bioavailability of the antioxidant flavonoid quercetin from various foods in man, FEBS Letters 418 (1997) 152–156. https://doi.org/10.1016/s0014-5793(97)01367-7.

[2] J.M. Geleijnse, L.J. Launer, D.A. Van Der Kuip, A. Hofman, J.C. Witteman, Inverse association of tea and flavonoid intakes with incident myocardial infarction: the Rotterdam study, Am J Clin Nutr 75 (2002) 880–886. https://doi.org/10.1093/ajcn/75.5.880.

[3] S. Fiorucci, J. Golebiowski, D. Cabrol-Bass, S. Antonczak, Oxygenolysis of flavonoid compounds: DFT

description of the mechanism for quercetin, Chem Phys Chem 5 (2004) 1726–1733. https://doi.org/10.1002/cphc.200400186.

[4] National center for biotechnology information. PubChem compound summary for CID, 5280343, Quercetin, https://pubchem.ncbi.nlm.nih.gov/compound/5280343 (accessed September 17, 2024).

[5] A.V. Anand David, R. Arulmoli, S. Parasuraman, Overviews of Biological importance of Quercetin: A bioactive flavonoid, pharmacogn Rev 10 (2016) 84–89. https://doi.org/10.4103/0973-7847.194044.

[6] P. Lakhanpal, D.K. Rai, Quercetin: A versatile flavonoid, Internet J Med Upd EJOURNAL 2 (2007). https://doi.org/10.4314/ijmu.v2i2.39851.

[7] Z. Dhaouadi, M. Nsangou, N. Garrab, E.H. Anouar, K. Marakchi, S. Lahmar, DFT study of the reaction of quercetin with and radicals, J Mol Struct: THEOCHEM 904 (2009) 35–42. https://doi.org/10.1016/j.theochem.2009.02.034.

[8] D. Jeevitha, K. Sadasivam, R. Praveena, R. Jayaprakasam, DFT study of glycosyl group reactivity in quercetin derivatives, J Mol Struct 1120 (2016) 15–24. https://doi.org/10.1016/j.molstruc.2016.05.003.

[9] M. Saranya, S. Ayyappan, R. Nithya, R.K. Sangeetha, A. Gokila, Molecular structure, NBO and HOMO–LUMO analysis of quercetin on single layer graphene by density functional theory.

[10] A. Karmakar, B. Singh, Spectroscopic analysis and theoretical investigation of hydrogen bonding interaction of quercetin with different acceptor molecules, J Mol Struct 1180 (2019) 698–707. https://doi.org/10.1016/j.molstruc.2018.12.034.

[11] Q. Aljelehawy, O.R. Mal Allah, G. Sourazur, Physicochemical properties medicinal chemistry toxicity and absorption of quercetin and its interaction with spike glycoprotein of SARS-CoV-2: Molecular docking, Nano Micro Bios 1 (2022). https://doi.org/10.22034/nmbj.2022.163207.

[12] S. Tortorella, M.M. Talamo, A. Cardone, M. Pastore, F. De Angelis, Benchmarking DFT and semi-empirical methods for a reliable and cost-efficient computational screening of benzofulvene derivatives as donor materials for small-molecule organic solar cells, J. Phys. Condens. Matter 28 (2016) 074005. https://doi.org/10.1088/0953-8984/28/7/074005.

[13] T.R. Paneru, M.K. Chaudhary, P. Tandon, B.D. Joshi, B.P. Bezerra, A.P. Ayala, Spectroscopic (FT-IR and FT-Raman) and quantum chemical study on monomer and dimer of benznidazole from DFT and molecular docking approaches, Heliyon 11 (2025) e42104. https://doi.org/10.1016/j.heliyon.2025.e42104.

[14] T.R. Paneru, M.K. Chaudhary, P. Tandon, T. Chaudhary, B.D. Joshi, Theoretical study on molecular stability, reactivity, and drug potential of cirsilineol from DFT and molecular

docking methods, Chem Phys Impact 8 (2024) 100641. https://doi.org/10.1016/j.chphi.2024.100641.

[15] P. Hohenberg, W. Kohn, Inhomogeneous electron Gas, Phys. Rev. 136 (1964) B864–B871. https://doi.org/10.1103/PhysRev.136.B864.

[16] M.J. Frisch, G.W. Trucks, H.B. Schlegel, G.E. Scuseria, M.A. Robb, J.R. Cheeseman, G. Scalmani, V. Barone, B. Mennucci, G.A. Petersson, H. Nakatsuji, M. Caricato, X. Li, H.P. Hratchian, A.F. Izmaylov, J. Bloino, G. Zheng, J.L. Sonnenberg, M. Hada, M. Ehara, K. Toyota, R. Fukuda, J. Hasegawa, M. Ishida, T. Nakajima, Y. Honda, O. Kitao, H. Nakai, T. Vreven, J.A. Montgomery, J.E. Peralta, F. Ogliaro, M. Bearpark, J.J. Heyd, E. Brothers, K.N. Kudin, V.N. Staroverov, R. Kobayashi, J. Normand, K. Raghavachari, A. Rendell, J.C. Burant, S.S. Iyengar, J. Tomasi, M. Cossi, N. Rega, J.M. Millam, M. Klene, J.E. Knox, J.B. Cross, V. Bakken, C. Adamo, J. Jaramillo, R. Gomperts, R.E. Stratmann, O. Yazyev, A.J. Austin, R. Cammi, C. Pomelli, J.W. Ochterski, R.L. Martin, K. Morokuma, V.G. Zakrzewski, G.A. Voth, P. Salvador, J.J. Dannenberg, S. Dapprich, A.D. Daniels, Ö. Farkas, J.B. Foresman, J.V. Ortiz, J. Cioslowski, D.J. Fox, Gaussian 09 Revision, 121 Gaussian Inc., Wallingford CT, Revision, (2009).

[17] A.D. Becke, Density-functional thermochemistry. III. The role of exact exchange, J Chem Phys 98 (1993) 5648–5652. https://doi.org/10.1063/1.464913.

[18] T.H. Dunning, Gaussian basis sets for use in correlated molecular calculations. I. The atoms boron through neon and hydrogen, J Chem Phys 90 (1989) 1007–1023. https://doi.org/10.1063/1.456153.

[19] R.F.W. Bader, Atoms in molecules: a quantum theory, Clarendon Press ; Oxford University Press, Oxford [England] : New York, 1994.

[20] T.A. Keith, AIMALL version (19.10.12) TK Gristmill software, Overland park KS. USA, (2019). http://aim@tkgristmill.com/.

[21] A. Frisch, A.B. Nielson, A.J. Holder, GaussView User Manual, Gaussian Inc., Pittsburgh, PA (2005) 556.

[22] T. Lu, F. Chen, Multiwfn: A multifunctional wavefunction analyzer, J Comput Chem 33 (2012) 580–592. https://doi.org/10.1002/jcc.22885.

[23] W. Humphrey, A. Dalke, K. Schulten, VMD: Visual molecular dynamics, J Mol Graph 14 (1996) 33–38. https://doi.org/10.1016/0263-7855(96)00018-5.

[24] N.M. O'boyle, A.L. Tenderholt, K.M. Langner, cclib: A library for package-independent computational chemistry algorithms, J Comput Chem 29 (2008) 839–845. https://doi.org/10.1002/jcc.20823.

[25] P. Banerjee, E. Kemmler, M. Dunkel,

R. Preissner, ProTox 3.0: a webserver for the prediction of toxicity of chemicals, Nucleic Acids Res (2024) gkae303. https://doi.org/10.1093/nar/gkae303.

[26] A. Daina, O. Michielin, V. Zoete, SwissADME: a free web tool to evaluate pharmacokinetics, drug-likeness and medicinal chemistry friendliness of small molecules, Sci Rep 7 (2017) 42717. https://doi.org/10.1038/srep42717.

[27] O. Trott, A.J. Olson, AutoDock Vina: Improving the speed and accuracy of docking with a new scoring function, efficient optimization, and multithreading, J Comput Chem 31 (2010) 455–461. https://doi.org/10.1002/jcc.21334.

[28] Discovery Studio 4.5 Guide, Accelrys, Inc., San Diego (2009). http://www.accelrys.cm.

[29] S. Domagala, P. Munshi, M. Ahmed, B. Guillot, C. Jelsch, CCDC 814512: Experimental crystal structure determination, (2011). https://doi.org/10.5517/CCWBKLB.

[30] C.F. Matta, R.J. Boyd, eds., The quantum theory of atoms in molecules: From solid state to DNA and drug design, 1st ed., Wiley, 2007. https://doi.org/10.1002/9783527610709.

[31] I. Rozas, I. Alkorta, J. Elguero, Behavior of ylides containing N, O, and C atoms as hydrogen bond acceptors, J Am Chem Soc 122 (2000) 11154–11161. https://doi.org/10.1021/ja0017864.

[32] E.R. Johnson, S. Keinan, P. Mori-Sánchez, J. Contreras-García, A.J. Cohen, W. Yang, Revealing noncovalent interactions, J Am Chem Soc 132 (2010) 6498–6506. https://doi.org/10.1021/ja100936w.

[33] G. Saleh, C. Gatti, L. Lo Presti, Non-covalent interaction via the reduced density gradient: Independent atom model vs experimental multipolar electron densities, Comput Theor Chem 998 (2012) 148–163. https://doi.org/10.1016/j.comptc.2012.07.014.

[34] Z. Jia, H. Pang, H. Li, X. Wang, A density functional theory study on complexation processes and intermolecular interactions of triptycene-derived oxacalixarenes, Theor Chem Acc 138 (2019) 113. https://doi.org/10.1007/s00214-019-2502-6.

[35] J.S. Murray, P. Politzer, Electrostatic Potentials: Chemical Applications, in: P. Von Ragué Schleyer, N.L. Allinger, T. Clark, J. Gasteiger, P.A. Kollman, H.F. Schaefer, P.R. Schreiner (Eds.), Ency Comput Chem, 1st ed., Wiley, 1998. https://doi.org/10.1002/0470845015.cca014.

[36] P. Politzer, D.G. Truhlar, eds., Chemical applications of atomic and Molecular electrostatic potentials: Reactivity, structure, scattering, and energetics of organic, inorganic, and biological systems, Springer US, Boston, MA, 1981. https://doi.org/10.1007/978-1-4757-9634-6.

[37] M.K. Chaudhary, P. Prajapati, B.D. Joshi, Quantum Chemical Calculation

and DFT Study of Sitagliptin: Insight from Computational Evaluation and Docking Approach, J Nep Phys Soc 6 (2020) 73–83. https://doi.org/10.3126/jnphyssoc.v6i1.30553.

[38] F.R. B., J.C. Prasana, S. Muthu, C.S. Abraham, Molecular docking studies, charge transfer excitation and wave function analyses (ESP, ELF, LOL) on valacyclovir : A potential antiviral drug, Comput. Bio Chem 78 (2019) 9–17. https://doi.org/10.1016/j.compbiolchem.2018.11.014.

[39] T. Chaudhary, M.K. Chaudhary, B.D. Joshi, Topological and Reactivity Descriptor of Carisoprodol from DFT and Molecular Docking Approach, J Inst Sci Tech 26 (2021) 74–82. https://doi.org/10.3126/jist.v26i1.37828.

[40] T.R. Paneru, M.K. Chaudhary, P. Tandon, B.D. Joshi, Cocrystal screening of benznidazole based on electronic transition, molecular reactivity, hydrogen bonding, and stability, J. Mol.Mod. (2024). https://doi.org/10.1007/s00894-024-06146-1.

[41] O. Kourat, A. Djafri, N. Benhalima, Y. Megrouss, N.E.H. Belkafouf, R. Rahmani, J.-C. Daran, A. Djafri, A. Chouaih, Synthesis, crystal structure, Hirshfeld surface analysis, spectral characterization, reduced density gradient and nonlinear optical investigation on (E)-N'-(4-nitrobenzylidene)-2-(quinolin-8-yloxy) acetohydrazide monohydrate: A combined experimental and DFT approach, J Mol Struct 1222 (2020) 128952. https://doi.org/10.1016/j.molstruc.2020.128952.

[42] R. Rijal, M. Sah, H.P. Lamichhane, H.S. Mallik, Quantum chemical calculations of nicotine and caffeine molecule in gas phase and solvent using DFT methods, Heliyon 8 (2022) e12494. https://doi.org/10.1016/j.heliyon.2022.e12494.

[43] T. Koopmans, Über die Zuordnung von Wellenfunktionen und Eigenwerten zu den Einzelnen Elektronen Eines Atoms, Physica 1 (1934) 104–113. https://doi.org/10.1016/S0031-8914(34)90011-2.

[44] R.G. Parr, R.G. Pearson, Absolute hardness: companion parameter to absolute electronegativity, J Am Chem Soc 105 (1983) 7512–7516. https://doi.org/10.1021/ja00364a005.

[45] R.G. Parr, L.V. Szentpály, S. Liu, Electrophilicity Index, J. Am. Chem. Soc. 121 (1999) 1922–1924. https://doi.org/10.1021/ja983494x.

[46] R.S. Mulliken, Electronic Population Analysis on LCAO–MO Molecular Wave Functions. I, J Chem Phys 23 (1955) 1833–1840. https://doi.org/10.1063/1.1740588.

[47] P. Jayavel, V. Ramasamy, N. Amaladoss, V. Renganathan, V.I. Shupeniuk, A facile synthesis, characterization, DFT, ADMET and in-silico molecular docking analysis of novel 4-ethyl acridine-1,3,9 (2,4,10H)-trione, Chem Phys Impact 8 (2024) 100476. https://doi.org/10.1016/j.chphi.2024.100476.

[48] C.A. Lipinski, Lead- and drug-like compounds: the rule-of-five revolution, Drug discovery today: Technologies 1 (2004) 337–341. https://doi.org/10.1016/j.ddtec.2004.11.007.

[49] L. Pinzi, G. Rastelli, Molecular Docking: Shifting paradigms in drug discovery, IJMS 20 (2019) 4331. https://doi.org/10.3390/ijms20184331.

[50] A. Daina, O. Michielin, V. Zoete, SwissTargetPrediction: updated data and new features for efficient prediction of protein targets of small molecules, Nucleic Acids Res 47 (2019) W357–W364. https://doi.org/10.1093/nar/gkz382.

[51] K.V. Ramana, Aldose reductase: new insights for an old enzyme, Bio Molecular Concepts 2 (2011) 103–114. https://doi.org/10.1515/bmc.2011.002.

[52] P.W. Rose, B. Beran, C. Bi, W.F. Bluhm, D. Dimitropoulos, D.S. Goodsell, A. Prlic, M. Quesada, G.B. Quinn, J.D. Westbrook, J. Young, B. Yukich, C. Zardecki, H.M. Berman, P.E. Bourne, The RCSB Protein Data Bank: redesigned web site and web services, Nucleic Acids Res 39 (2011) D392–D401. https://doi.org/10.1093/nar/gkq1021.